
Fractal Properties of Whitecaps

B.R. Kerman

*Atmospheric Environment Service
Canada Centre for Inland Waters
Burlington, Ontario L7R 4A6*

and

K. Szeto

*Department of Physics
University of Toronto
Toronto, Ontario*

[Original manuscript received 18 April 1991; in revised form 7 June 1994]

ABSTRACT *Images of a field of breaking waves over the ocean obtained using a line-scanner on an aircraft are analyzed for a possible fractal geometry. The cumulative probability function of the intensity is shown to be self-similar for sufficiently large intensities occupying about 10% of an imaged area. This structure is invariant to successive averaging over successively larger boxes. A box-counting technique was applied to images of one representative flight. The estimated fractal dimension decreases from about 2.25 for a 10% areal coverage to about 1.7 for 0.1% coverage. It is concluded that the spatial distribution of the scattered light from foam and whitecaps is not monofractal, but is instead multifractal.*

RÉSUMÉ *On analyse les images d'un champ de vagues marines déferlantes provenant d'un balayeur linéaire aéroporté afin de trouver une géométrie fractale. On montre que la fonction de probabilité cumulative de l'intensité est autosemblable pour des intensités assez grandes occupant près de 10 % d'une image. La structure est invariante pour un moyennage successif utilisant des boîtes de plus en plus grandes. On a appliqué une technique de comptage de boîtes aux images provenant d'un vol représentatif. La dimension fractale estimée diminue d'environ 2,25 pour une couverture de 10 % à près de 1,7 pour une couverture de 0,1 %. On peut conclure que la distribution spatiale de la lumière diffusée par l'écume et les moutons n'est pas monofractale, mais plutôt plurifractale.*

1 Introduction

Wave breaking over the ocean in a wind-wave field plays an important role in controlling some physical processes at the air-sea interface. Dynamically, an equilibrium is thought to exist between the input energy from the wind forcing on the

waves and the ultimate dissipation of that energy by the creation of turbulence in the breaking waves (Phillips, 1985). Accordingly, breaking waves are localized centres of dissipation whose local turbulence results from the atmosphere's momentum near the ocean surface, and hence acts as a drag on the atmosphere.

The entrainment associated with the breaker's turbulent turnover produces bubbles that are carried below the surface for possible dissolution or gaseous accretion, depending on the size distribution of the bubble cloud and the saturation level of gas in the water. This mechanism may provide, therefore, for an exchange process for the transfer of gases between the atmosphere and ocean (for example, Thorpe, 1982; Kerman, 1984; Kitaigorodskii, 1984; Csanady, 1990).

Upon their return to the surface the bubbles either remain stabilized in a foam patch or rupture, carrying in their vertical jet a thin skin enriched with the particles collected by impact scavenging during their rise (MacIntyre, 1968; Blanchard, 1983). The enrichment of aerosols associated with the ejected droplet, resulting from partial evaporation, is thought to be important (Buat Menard, 1986) in maintaining a source of salt-laden cloud condensation nuclei, as well as interfacial fluxes of trace constituents, including bacteria, viruses, heavy metals, radioactivity and inert organic material (Kerman, 1986).

Of interest in ocean acoustics is the generation of sound at the surface associated with bubbles produced both as single units and as a spongy cloud (Kerman, 1988). A source of bubbles close to the surface alters the bulk modulus of the upper metres of the ocean leading to ducting (Farmer and Vagle, 1989), attenuation (Novarini and Bruno, 1982) and scattering (Crowther, 1980) of propagating sound.

The presence of foam and bubbles at the surface alters the reflectivity properties of the ocean surface. In the case of light (Austin and Moran, 1974) additional multiple scattering occurs from a matrix of randomly layered specular surfaces. If the surface is illuminated by microwaves, wedge scattering may occur in addition to Bragg scattering.

Breaking waves also play a significant role in effects as diverse as the evaporation from the oceans and the evaluation of forces on structures in ocean engineering. The proceedings of several recent workshops (Monahan and MacNiocaill, 1986; Monahan and Van Patten, 1989) contain numerous other references to the ubiquitous role of breaking waves at the air-sea interface.

The incorporation of wave breaking effects in these different applications often utilizes the concept of a statistically steady fractional coverage, i.e. the areal extent of the process, at the sea surface at a given time. This description is related to a combination of factors – the number of waves breaking in a given area in an interval of time, the average size of the breakers as well as the average duration of each event. The measurement of these several descriptors is difficult for several reasons. From the operational point of view it is demanding, in a hostile environment, to gather voluminous data of both wide areal extent, and fine spatial and temporal resolution. From the analytical point of view, the principal difficulty arises from trying to represent the highly variable texture of the surface.

Recently Glazman and Weichman (1989) have proposed a statistical geometric description of the ocean surface in terms of its wave height and slope spectra. In such a description it is thought that the spatial geometric description of the production of instabilities, associated interchangeably with wave slope and vertical wave acceleration, in some sense should be equivalent to the spatial distribution of the breaking waves and their local turbulence.

Monahan (e.g. Monahan and O'Muircheartaigh, 1986) has studied many of these aspects, particularly the extent and duration, of breaking waves in some detail. Other studies have been reported by Toba and Chaen, 1973; Ross and Cardone, 1974; Snyder et al., 1983; Longuet-Higgins and Smith, 1983; Weissman et al., 1984; and Holthuijsen and Herbers, 1986. One objective of such studies has been to parametrize the areal extent of the breaking waves in terms of the near-surface wind speed, air-water temperature difference, salinity and water temperature. Another major thrust has been to relate the occurrence of whitecaps, hereafter considered as those areas of active entrainment in the life cycle of breaking waves, to a critical wave steepness.

Techniques to estimate the whitecap coverage are usually based on ship- or buoy-based photographic observations, with some aircraft-based measurements (Ross and Cardone, 1974; Smith, 1981) having been reported. The first, and we believe still unresolved, problem common to any measurement strategy is how to make an unambiguous estimate of what constitutes whitecaps, i.e. active aeration, and what fraction of the image to ascribe to foam, i.e. stabilized bubble rafts. One is usually presented with what at first seems a simple black and white image. At closer inspection one begins to ask how to differentiate between weak entrainment and bright foam, and between specular reflection and weak unresolved foam or subsurface bubble clouds.

The question can be answered operationally, and with considerable care one is able to compare data treated similarly. But so far as we are aware, neither have the techniques been based on some stated reflectivity properties nor have the methods that have been used been able to estimate their error owing to unresolved bubble-related elements. In the context of remote sensing the problem is the familiar one of identification and classification. The typical statistical scatter in estimated coverage, say as a function of wind speed, originally motivated a search for a definitive algorithm to classify these various features of a breaking wave field from digitized images of a wind-swept sea.

The study to be described here evolved from one of making a more precise estimate of whitecap coverage based on extensive surface interrogation into a contribution of providing an unambiguous statement of the constitutive properties of whitecaps and foam. In other words, how does one recognize a whitecap within the imagery? Our analysis is limited primarily to some unique physical and geometric properties of the multi-spectral images. As will be shown, each provides new insights into the basic optical and hydrodynamical processes occurring on the surface.

There is also an aspect of the work that falls broadly under the umbrella of human consciousness and artificial intelligence. The connection between the geometric properties of the sea in the presence of breaking waves and the meteorological characterization, primarily by the wind speed, has been utilized by sailors probably from before recorded history. When in the nineteenth century Admiral Beaufort originally codified the wind forcing, it was in terms of the sailing characteristics of naval frigates to enable better wind reporting and accountability of sailing ships. Gradually, as a result of the adoption of steam in place of wind for propulsion, the method of reporting evolved into a characterization of the state of the sea surface. Today so-called Beaufort scales 5 and larger utilize primarily the presence, extent and texture of breaking waves to indicate sea state.

The imagery of whitecaps extends beyond the practical to the artistic and perhaps to the human psyche. Any casual survey of oceanic or shoreline seascapes soon reveals the interest that the artists, and presumably the viewers, have in capturing the violence and unexpected diversity of breaking waves. Why the human mind should be fascinated by such images may lie in the challenge to codify such wildly fractured, yet somehow ordered, shapes. Other similarly interesting subjects in our predilection for landscapes include objects such as trees, forests, mountains and streams, all displaying characteristics that are now classified as examples of natural fractal geometry (Mandelbrot, 1983).

The fleeting nature of a breaking wave may add yet another challenge to the human intellect to codify the process. That there exists a look-up table, long accepted as valid, that relates the decoding of an entire scene to a single number, motivates us to believe that there exists an underlying fractal description that can ultimately be related to the wind, or equivalently to the near-surface hydrodynamics.

As is now well known, in recent years the study of the geometry of naturally occurring fractured objects has been given impetus by the introduction of modern geometrical concepts to science by Mandelbrot. Viewed in a deterministic framework, fractal geometry provides a description of geometrical identities that are repeatedly split or reoriented in a cascade fashion. Hence the number of points or line elements or closed figures present at the current step in an iterated procedure, such as in a decimation or splitting cascade, is proportional to the number at the previous step, which itself is proportional to the number at the yet previous step. Accordingly, a logarithmic relationship is to be expected between the number of elements of the given size and their size.

Viewed in a probabilistic sense, which is the sense of fractal geometry followed in this study, the cascade process is governed by a birth/death process that prescribes only the probability of an occurrence of some event or configuration. For example, the number of school-age children is described by probabilities associated with marriage, fertility and infant mortality. A logarithmic relationship again arises and can be formulated basically as the number of occurrences beyond a sampled level or count, i.e. exceedances, in terms of age. The attractiveness of the application of fractal geometry to a physical process such as breaking waves is the rather naive

belief that the process may be essentially described by a single exponent, referred to very loosely as the fractal dimension. (A more explicit formulation is offered in Section 3.) Another feature of such analytic descriptors as fractals stems from the realization that the determination of these geometric characteristics generally does not specify a unique dynamically predestined generating procedure. At first exposure the lack of any clear relationship to classically instilled physical intuitions seems to offer little. The reward comes in applying a totally different set of concepts to complement both known results and theoretical models, as well as to provide new insights.

New concepts arise – Why is the sea surface like a classical Brownian process? What would be the equivalent birth/death description? What iterative physical process is involved to produce the statistical geometry of a wind-swept sea?

2 Experiment and imagery

A multi-spectral scanner was flown on board a DC3 aircraft of the Canada Centre for Remote Sensing over the Atlantic Ocean to the south and east of Halifax, Nova Scotia, and over the northeast portion of the Bay of Fundy. A total of 12 sorties were flown between 23 and 29 March 1984. An image was built up as a sequence of cross-flight lines. Each sortie was flown at a height of about 500 m, the elevation required to achieve contiguous, non-overlapping coverage of neighbouring lines. Aircraft orientation was selected to minimize glint into the laterally scanning spectral radiometer. The actual data recording lasted about 10 min, which at a design wind speed of 10 m s^{-1} and an aircraft ground speed of 50 m s^{-1} , roughly equates to 1 h of fixed point sampling on the surface. Wind speeds ranged from 6 to almost 20 m s^{-1} , as estimated both by the pilots and by observers at neighbouring land sites.

The optical modulation transfer function of the line-scanner rolls off with decreasing scale to a minimum response for a field of view of about 2.5 mrad. From a height of about 500 m the spatial resolution of the imaged surface is about 1 m. The swath width was limited to the central 512 pixels in each line, and hence a width of about 0.5 km, whereas the image length was about 30 km.

The spectral bands of the scanner were centred at 0.57, 0.67, 0.73, 0.83, 0.95 and $1.64 \mu\text{m}$ with an average bandwidth to centre wavelength of about 15%. The equipment and its calibration is described more fully by Zwick et al. (1980). Several television cameras, one a low light-level model sensitized to the near infrared, were also carried on board in an attempt to estimate the age of whitecaps while they were encountered by the imaging scanner.

An example of a flight (7), over the Bay of Fundy on 25 March at about 1400 LST, is given in Fig. 1. The aircraft heading was 46° and the wind direction was between 265 and 300° . Winds reported nearby, but somewhat downwind, at Greenwood, were 10 m s^{-1} with gusts to 15 m s^{-1} while upwind at St John they were reported as 8 m s^{-1} with gusts to 12 m s^{-1} . The pilots who had flown many sorties over the ocean and had experience in categorizing the sea state, estimated the overwater

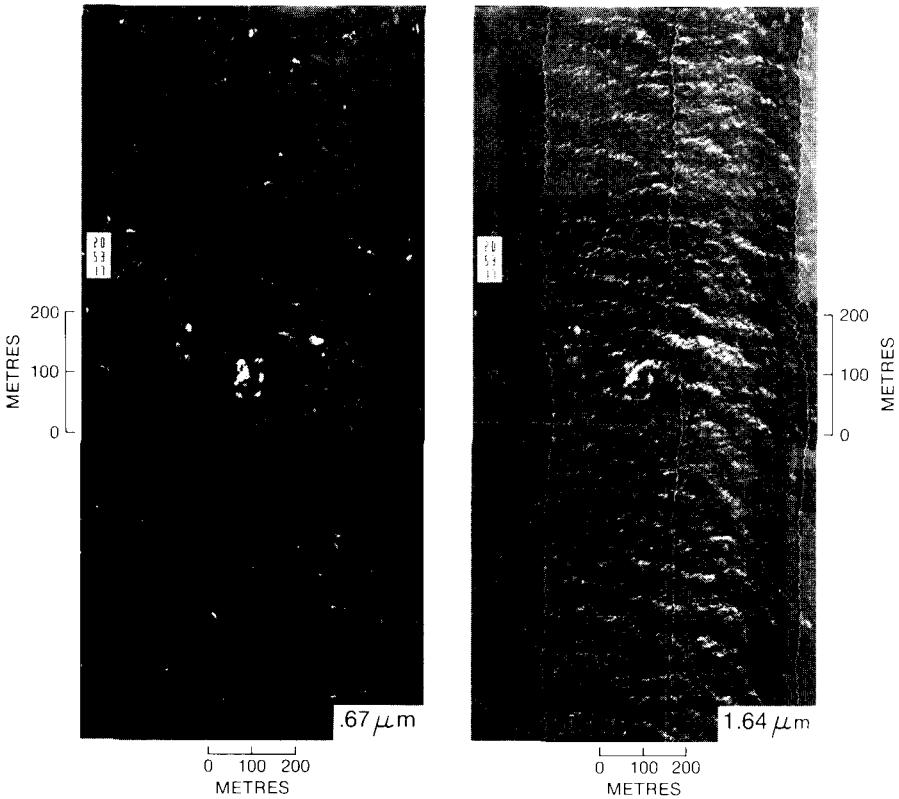


Fig. 1 Uncorrected image of flight 7 on 25 March 1984 over the Bay of Fundy, displaying two channels (0.67 and 1.64 μm). The direction of the aircraft is along the principal axis. The sun illumination is from behind the aircraft and the wind is blowing from the lower left.

winds at 15 m s^{-1} with gusts to 18 m s^{-1} . The sun was located in the direction of about 210° for that date and hour. The aircraft height was 430 m and its ground speed, about 66 m s^{-1} .

Two spectral bands have been chosen to demonstrate the characteristics of the images. The first at $0.67 \mu\text{m}$ is typical of all images seen through filters ranging from the orange to the invisible far red at about $1 \mu\text{m}$, although optimum contrast occurs near $0.95 \mu\text{m}$. The second image at $1.64 \mu\text{m}$, is perhaps the first image of a wind-driven sea to be captured at such a wavelength, to the authors' knowledge. (The thin wavy vertical continuous lines are electronic noise.)

Several interesting features can be seen in the images. The first is that of local bright regions associated with the whitecaps. Their size varies over almost an order of magnitude. Their shapes as captured in the imagery are complex, varying from

small individual, presumably underresolved, patches to an ensemble of closely spaced and geometrically arranged patches. Examination of the background of the 0.67- μm image reveals a degree of milkiness that corresponds to rather distinct banding in the 1.64- μm image. Further, a comparison of the major whitecap event in the centre of the image reveals that the event is distinctly less pronounced in the 1.64- μm image.

The 1.64- μm wavelength image also reveals structure that was not evident in the visible, at least without enhancement. Bands appear that are aligned primarily across the mean wind direction, here orientated from the lower left to upper right in the image. A closer inspection of individual bands reveals a tendency for narrow streaks within these bands that are in turn aligned with the wind direction. This apparent within-band arrangement is lost, however, if the image is examined at too small a field of view. In addition, a re-examination of the whitecaps, based on a larger sample than presented, reveals that the major axis of the whitecaps tends to be aligned across the wind direction, with fine structure streak lines running with the wind.

The streaks appear to have characteristics similar to those analyzed by Koepke (1984). Typically, although the width of the crosswind bands is about 15 m, with band-to-band separation in the wind direction of about 70 m, there is considerable variation particularly towards narrower bands composed of individual well defined streaks extending on the order of only 5 m, with band-to-band distances of the order of 50 m in the wind direction. Several clearly aligned streaks are separated by a distance about equal to the width of the band in which they are contained. Judging from Koepke's photographs, the streaks appearing in our imagery may be comparable to or thinner than the limit of scanner resolution of about 1 m.

3 Fractal geometry: Properties and techniques

In order to understand the basic concepts associated with fractal geometry, let us consider the extension of the classical mathematical analysis of continuous functions which, contrary to normal practice, is assumed to be non-differentiable almost everywhere or equivalently differentiable almost nowhere. Our presentation follows that of Rothrock and Thorndike (1980) with considerable distillation. We also begin with a consideration of functions in 1 dimension and extend to 2 dimensions as a natural extension to evaluate our 2-D images.

The definition of a continuous function, $f(x)$, is one for which

$$\lim_{\Delta \rightarrow 0} [f(x + \Delta) - f(x)] = 0 \tag{1}$$

For the function to be differentiable the limit of the ratio of the differences of both the function and its argument must exist, i.e.

$$-\infty < \lim_{\Delta \rightarrow 0} \frac{[f(x + \Delta) - f(x)]}{\Delta} < \infty \tag{2}$$

If this limit process does not exist in the location of a given value of x , it is possible that a more general limit condition does exist, the so-called Lipschitz condition where

$$-\infty < \lim_{\Delta \rightarrow 0} \frac{[f(x + \Delta) - f(x)]}{\Delta^\alpha} < \infty \quad (3)$$

for $0 < \alpha < 1$. In essence the parameter α , called the Lipschitz exponent, is a measure of how much one must warp by expansion the x dimension to achieve a bounded ratio in the limit. It is intimately related to the "roughness" of the function, which is related to both the severity and the density of points where a derivative does not exist. For $\alpha = 0$, the function f is discontinuous (Eq. (1) is violated) whereas for $\alpha = 1$, f is both continuous and differentiable.

The equivalent question of the existence of a Lipschitz condition when f is a realization of a random non-differentiable process can be expressed in terms of the variance, i.e. for

$$\sigma^2(\delta f) = E[f(x + \Delta) - f(x)]^2 \rightarrow \Delta^{2\alpha} \quad (4)$$

where E is the expectation operator and the symbol \rightarrow denotes how the right-hand side varies as a limit (for example, as an average of many points or sampled sub-functions) is approached. Often Eq. (4), for example, in the study of turbulence, is referred to as the structure function of the random process. When such functions exist, they are associated with a spectrum, $\Phi(\kappa)$, which at large wavenumber κ asymptotically approaches a form $\kappa^{-\beta}$ where

$$\beta = 2\alpha + 1 \quad (5)$$

For example, in Kolmogorov's classical expressions for large Reynolds number turbulence, $\alpha = 1/3$, and $\beta = 5/3$. Although (5) has not been proved rigorously by mathematicians, no examples exist to contradict its validity. An alternative relationship in terms of the classical correlation function, $R(\Delta) (= E[f(x + \Delta)f(x)])$, is given by

$$R(0) - R(\Delta) \rightarrow \Delta^{2\alpha} \quad (6)$$

as $\Delta \rightarrow 0$.

Implicit in the Lipschitz condition for a random function is the concept of self-similarity – that is, the statistics of the geometrical structure are only a function of scale. If a subset of a sampled function, f , sampled at an interval, Δ , was examined for the expected square differences between successive samples, the result would be identical to that for another sampled function, at say 2Δ , to within a factor $2^{2\alpha}$. Alternatively, if the second sampled function is multiplied first by $2^{-2\alpha}$, and the differences computed at 2Δ , then the second function would be indistinguishable from the first – probabilistically. The self-similarity condition can be expressed as

$$\Pr[\delta f(\lambda\Delta) > \delta f^*] = \Pr[\lambda^\alpha \delta f(\Delta) > \delta f^*] \tag{7}$$

that is, the cumulative probability functions of the variously sampled and amplitude-modified functions are identical. δf^* is simply the increment in δf for which the cumulative probability function (hereafter cpf) is tested.

Another method developed by geometers for characterizing continuous but almost everywhere non-differentiable functions utilizes the concept of coverings. Consider a set of points arranged on a line. Consider the number of intervals of length, Δ , needed to be placed over (cover) the points. If the points were in some ordered arrangement, such that the nearest neighbours were separated by more than Δ and there was no possibility of clustering for a sufficiently small Δ , the number of the intervals needed to cover the points would be the same for all interval lengths less than Δ . However, if the points were not ordered and, in particular, if there was no limit to the clustering, in the sense that no matter how small Δ became, there was a measurable probability of finding multiple points in an interval, the number of intervals required for the covering is then a function of Δ . If, and only if,

$$n(\Delta) \rightarrow \Delta^{-D} \tag{8}$$

that is, the number of intervals in a covering is a power law in some exponent, D , (not necessarily an integer) then the process (here a set of distributed points) is defined as having a Hausdorff or fractal dimension, D . Generally a process defined by its geometric realizations is defined to be fractal if its Hausdorff dimension exceeds its Euclidean dimension. Here the Euclidean dimension of a set of (well ordered) points or a single point is 0. Such a result can be recovered from (8) noting the constancy of the counts needed for the covering, whatever the interval size up to some maximum. It is the ability of the Hausdorff dimension to characterize the otherwise seemingly indescribable disorder that makes the concepts of a fractal process so valuable.

Let us now consider what is often called the “shoreline problem” where a closed perimeter is unwrapped and represented as a one-dimensional function over an interval $[0, 1]$. When applied to the one-dimensional random function, f , the average number of intervals needed to cover an increment of the function $|\delta f(\Delta)|$ ($= |f(x + \Delta) - f(x)|$) is its average distance, Δ^α , from Eq. (4), divided by the length of the interval, Δ , i.e. $\Delta^{\alpha-1}$. For an overall length of unity, there will be Δ^{-1} intervals contributing to the covering so that the number of intervals required is

$$n(\Delta) \rightarrow \Delta^{-1} \Delta^{\alpha-1} \rightarrow \Delta^{\alpha-2} \tag{9}$$

From Eq. (8), it is now possible to relate the fractal dimension to the Lipschitz exponent, i.e.

$$D = 2 - \alpha \tag{10}$$

or to the spectral exponent (Eq. (5))

$$\beta = 5 - 2D \quad (11)$$

These interrelationships are significant in that they provide for a variety of techniques to estimate the fractal dimension or infer the spectral structure. For example, a covering method provides an estimate for the length, L , of a random function sampled over a unit interval at increments, Δ , given by

$$L(\Delta) = \Delta n(\Delta) \rightarrow \Delta^{1-D} \quad (12)$$

as $\Delta \rightarrow 0$. In terms of Eq. (6) this relationship can be rewritten

$$L(\delta) \rightarrow \Delta^{-1}[R(0) - R(\delta)]^{1/2} \quad (13)$$

which allows for the direct calculation of the length of a "rough" function in terms of the function's low-order spatial statistics.

Several other useful properties of random functions have also been examined by Rothrock and Thorndike (1980). The expression for the probability of crossing a given level f^* of a function f in an interval Δ is

$$\Pr(f^*; \Delta) \rightarrow H(f^*)\Delta^{1-D} \quad (14)$$

where $H(f)$ is the cpf of f . By extension, if an interval of size Δ is used to cover the interval, the number of counts exceeding a threshold will vary according to (14) as Δ^{1-D} where $1 < D < 2$.

Consider now a 2-dimensional covering of the same shoreline by boxes of side length Δ . The number of boxes required is

$$n_2(\Delta^2) \approx \Delta^{-2}\Delta^{\alpha-1} \quad (15)$$

by the same arguments that lead to Eq. (9). Hence we are led to a general relationship between fractal dimension and Lipschitz exponent

$$D = E + 1 - \alpha \quad (16)$$

where E is the imbedding dimension (2 for images). The Lipschitz exponent, α , is in both cases (for the line and surface) a co-dimension, that is, the difference between the imbedding Euclidean dimension (1 or 2) incremented by 1 and the appropriate (Hausdorff) fractal dimension of the random set of points ($0 < D < 1$) or line ($1 < D < 2$). It is invariant to our method of covering the function's support, i.e. whether coverings in 1 or 2 dimensions are involved.

In the next section we apply some of these concepts and techniques to estimate the fractal properties of the images described in Section 2.

4 Analysis

A precondition for the existence of a fractal process is a wide separation between the inner and outer scales. Breaking waves occur with spatial dimensions from centimetres (microbreakers) to massive foam patches of the order of the energy-containing wavelength and to the spatial separation between events extending up to hundreds of metres. From casual observations from a ship or platform it can be observed that the spatial variability near foam patches and in the vicinity of active breakers ranges from millimetric sizes associated with bubbles to the outer size of the event itself. Both of these estimates lead to a scale ratio of outer to inner scale of the order of 10^3 – 10^4 , which gives us confidence that a fractal process can exist for breaking waves. However, the inner scale of the observations is set here by the minimum resolvable size determined by the optics of the line scanner, which is about 0.8 m^2 . Therefore the accessible range of scales is only 10^1 – 10^2 . However, as shown below there exists evidence of the scale invariant process over this range of scales.

In this section we will examine the data images in several ways to test for the presence of a consistent fractal structure. The analysis is not exhaustive. Other techniques exist, but they are considered here to be redundant. That is not to say they might not prove to be useful or even superior in some sense if they were further examined. However, a comparison of various techniques provided valuable information about the basic structure of the process as represented by the images – enough to conclude that the real problem lies elsewhere in describing a more complex situation than outlined in Section 3. A reasonably consistent result emerges from the existing ensemble of analyses.

a Cumulative Probability Function

The first technique applied to the data was an examination of each flight's cpf for the potential scaling structure. The results of 6 representative flights are presented in Fig. 2. It is noted that the cumulative probability is equivalent to the relative areal coverage, since it is based on counting those pixels whose intensity exceeds a given thresholded value, and comparing that number to the image's overall size expressed in pixels. The characteristics of the 6 flights are provided in Table 1.

Although the range of intensities varied between flights depending on a number of factors, including illumination, surface wind speed, optical acceptance angle and possibly air-sea temperature differences and dissolved organics, there is a well defined tendency for a power law structure in the cpf in all flights. The linear extent of the relationship is limited to subranges for flights 11 and 12. The steep slope of the cpf, varying approximately as I^{-3} , is dramatic evidence of the difficulty of providing a threshold scheme to identify whitecaps solely on the basis of reflectivity because of the sensitivity of the process. To emphasize this point we note that a 20% error in establishing a threshold intensity leads to over a 50% error in establishing the areal extent of the process. Further if the threshold light level varies in some

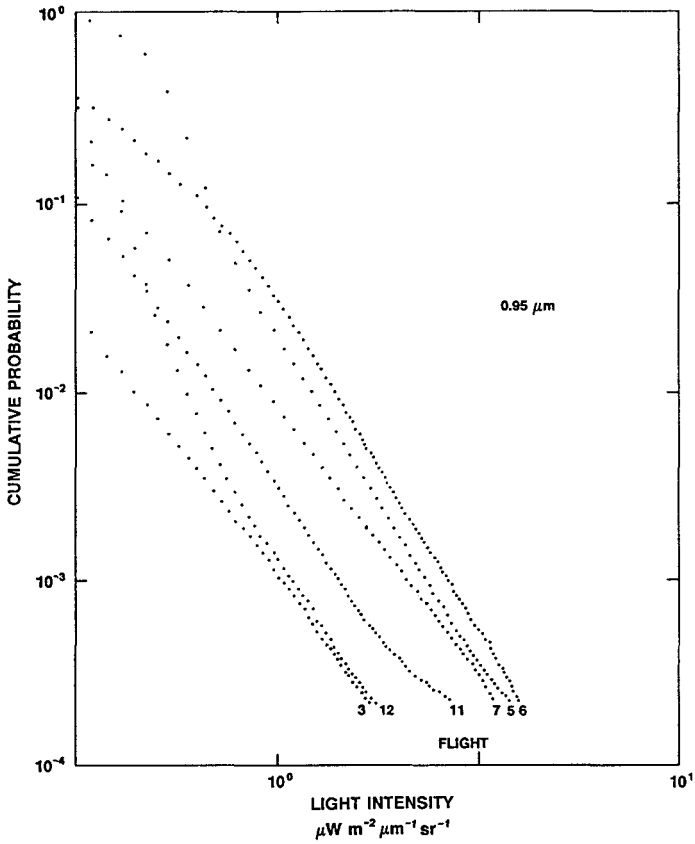


Fig. 2 Cumulative probability functions for all flights.

TABLE 1. Characteristics of 6 flights in March 1984

Flight	Date (March 1984)	Time (UTC)	Location (Bay of Fundy, Halifax)	Estimated Surface Wind Speed (m s^{-1})	Wind Direction (deg.)	Aircraft Heading (deg.)	Sun Direction re Aircraft Heading (deg.)
3	24	1856	B	14	290	-145	184
		1906					
5	25	1651	H	12	280	-90	181
		1700					
6	25	1741	B	17	275	55	3
		1747					
7	25	1752	B	17	275	-135	165
		1759					
11	28	1531	H	9	310	-30	183
		1540					
12	29	1522	B	19	55	60	174
		1535					

sense approximately linearly with wind speed one immediately obtains a cubic dependence of areal extent on wind speed.

Flight 6 was made directly into the sun and resulted in both a more intense image and one of distinctly different probabilistic structure compared with flight 7 taken minutes later while flying away from the sun. Further analysis revealed a tendency for other flights to have the slope of flight 6 or 7 depending on whether the aircraft was aligned with a significant projection of its flight vector into or with the wind. The slopes of the cpf of the different flights with the wind (3, 7) are somewhat less steep indicating more intense pixels, for a given total illumination and reflection, on the average than flights into the wind (6, 11, 12). Shadowing effects are discounted because of the aircraft height (about 400 m). If there was an effect due to the tilt of the breaking waves on their front faces it would contribute to the into-wind flights, which is contrary to the observations.

It is hypothesized that the varying sensitivities in Fig. 2 arise from the angular properties of light scattered by bubbles (Davis, 1955) on or near the surface. Flights 3 and 7 have a significant component of the sun's direction in the wind direction so that the sensor would be receiving primarily light scattered in a forward direction. Conversely flights 11 and 12 were collecting backscattered light. Flight 5 is illuminated across-wind and would be receiving backscattered light.

Flight 6, although definitely receiving forward scattered light, has a cpf slope that more closely resembles the slopes of backscattered cases. The reason for this is believed to be the contribution from spectral reflections that first appear as a broad hump near an areal coverage of about 0.08 and distort the slope overall. The hump is unique to flight 6, the only flight into the sun.

The conclusion to be drawn from the cpfs of the various flights is that a scaling structure does exist in intensity. Further the details of the scaling process depend on whether forward or backward scattered light is observed. It is worth emphasizing that the scaling structure by itself does not prove the existence of a fractal process, which can only be determined by imposing some form of a cascaded spatial transformation. In the subsequent analysis, flight 7 is examined almost exclusively because of its overall larger intensity arising from more intense illumination than experienced in flights 3, 11 and 12, and more breaking waves owing to the higher wind speed as well as its forward scattered orientation.

Another interesting property of the cpf is the difference between the images at 0.95 and 1.64 μm as presented in Fig. 3. Clearly the 1.64- μm image cpf is steeper, and the expected range of intensities is reduced. This effect can be related to the wavelength and depth dependence of the reflectivity of foam and whitecaps (Whitlock et al., 1982). It is expected that the 1.64- μm response is sensitive to bubble density, so that with increasing thickness of the bubble scattering layer leading to multiple reflections, there is also noticeably more absorption than at wavelengths less than about 1 μm . This tendency to de-emphasize the thick region scattering (whitecaps) compared with the foam is clearly visible in the imagery. The further change in sensitivity at a coverage of 0.005 to a yet more uniform brightness

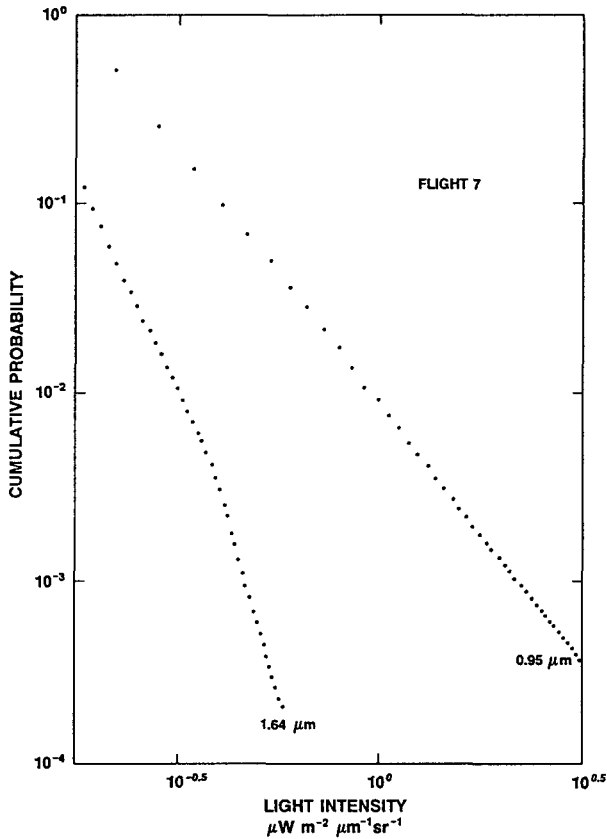


Fig. 3 Comparison of the cumulative probability functions for two channels of the image from flight 7.

indicates that almost no more scattered light is available for increasing thickness. Alternatively at some stage, here assumed to relate to larger breaking waves and the bubble layer thickness associated with a coverage of 0.005, absorption is almost equal to scattering.

b Degraded Resolution

From Eq. (14) the probability of encountering a given light level in a given interval is a function of Δ and the cumulative probability function. Accordingly an analysis was devised to investigate whether the average values of a function in a sequence of subintervals might also be distributed as a power law in Δ . Figure 4 presents an analysis of flight 7 in which the data have been successively averaged over squares of length (number of pixels) 1 to 32 i.e. 2^i for $i = 0$ to 5.

The most striking result is that the power law structure is maintained for a region involving the larger intensities. Clearly this range of intensity values is, except for

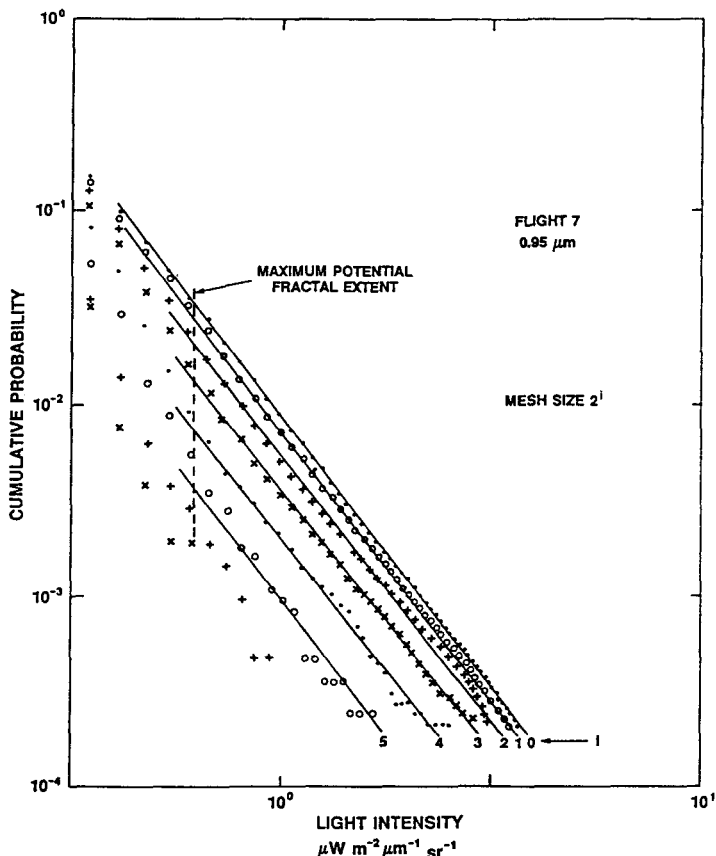


Fig. 4 Cumulative probability function of the 0.95- μm channel of flight 7 averaged over successively larger box sizes.

an amplitude effect, invariant to the scale of the averaging, and therefore potentially contains a fractal process.

The extent of the power law structure decreases monotonically with increasing average box size. In addition, the spacing between the decreasing cpfs increases with increasing box size. If the process was fractal as defined above, and if the averaging operator had the same properties as level crossing statistics, the separation between successive box sizes would be constant in Fig. 4. That it is not constant will be shown below, with hindsight, to be related to the failure of our hypothesis that the process has only one fractal dimension.

Nevertheless the process of degrading the resolution is useful in estimating the effect that the finite sample area (1 m^2) associated with the optical sensor has had on conditioning the statistics compared to an even finer resolution. An estimate of the maximum possible fractal extent was made by estimating the upper limit of the linear trend extending from the larger to lower intensities in Fig. 4 for flight 7

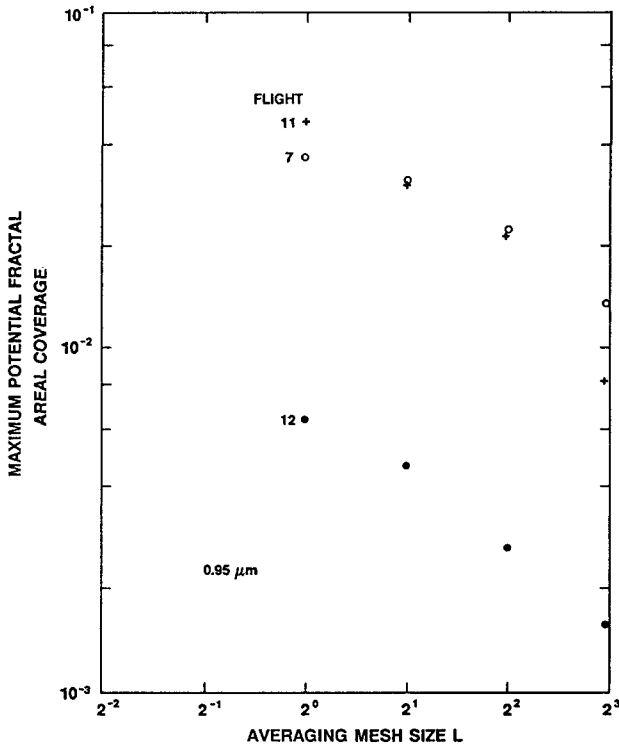


Fig. 5 Estimated maximum extent of fractal behaviour for different flights.

and similar graphs for several other flights. The results that are presented in Fig. 5 demonstrate that if $1/2$ or $1/4$ the available resolution were to have been available there would at most be a factor of 2 increase in estimated coverage in the low wind, large fetch case (flight 11) and considerably less in high wind, small fetch cases (flights 7 and 12).

It is known that whitecap coverage increases with both wind speed and fetch. For us to evaluate properly whether the estimates of the maximum extent of potential fractal structure is in fact whitecap coverage requires primarily a larger variability in fetch than the present dataset contains. Most data were taken within 75 km of the shore. In addition, several other factors may have an effect. As Thorpe (1986) has shown, the depth of the bubbling and the texture of the bubble clouds is governed by among other factors the presence of Langmuir cells and the atmospheric stability. In addition, the production of foam is a function of both the salinity, which affects interfacial forces on bubbles, and organic productivity, which affects the coating around the bubbles. The flights have a limited range of conditions of air-sea temperature contrast of no more than several degrees. The two locations for flights, southeast of Halifax and in the Bay of Fundy near Greenwood, may

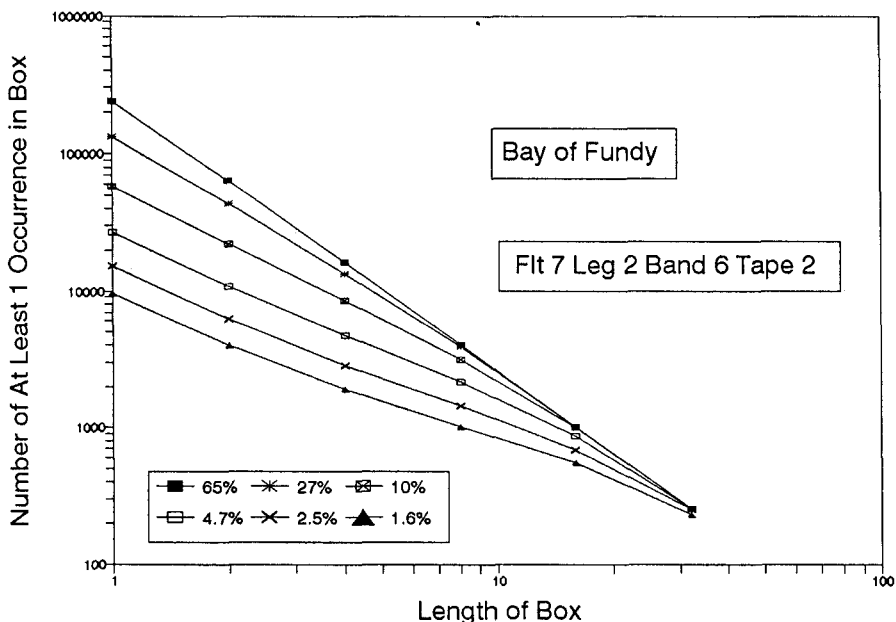


Fig. 6 Number of boxes (2^i) needed to cover image (flight 7, channel 0.95 μm) with a given box of size L .

conceivably differ modestly in organic composition and salinity associated with ocean currents.

c Coverings

The classical method of determining fractal properties, the covering technique, is applied here by counting the number of boxes of a given size, L , required to cover a set of subimages (points) produced by thresholding the image intensity at a value associated with a given areal extent (see Fig. 2). The results of this analysis for the 0.95- μm image of flight 7 are plotted in Fig. 6 for a range of coverage from 65 to 1.6%.

The main feature of Fig. 6 is its well defined linear relationship near the minimum resolution for as much as a decade of scale variation. The linear extent increases for coverages less than 10% and is apparently limited by the mean distance between isolated thresholded "islands". For box sizes comparable with and larger than the average distance to nearest neighbours, accepting the first occurrence of an above-threshold pixel also accepts not only all pixels in that box from the same island, but also any pixels from any overlapping island. This saturation effect is manifested in the -2 slope in the larger coverages in Fig. 6 for sufficiently large box size. Alternatively expressed, at a given threshold with a given spatial density of islands, when the box size becomes too large the box-covering analysis acts as if the image

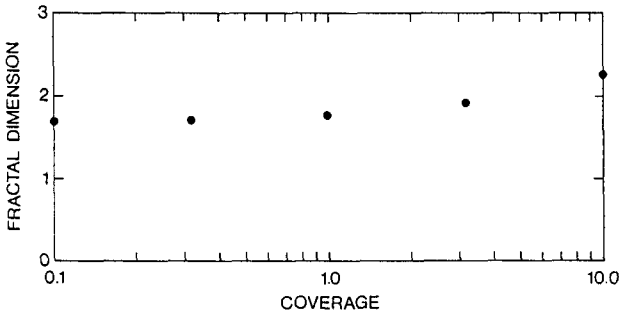


Fig. 7 Fractal dimension of flight 7 image thresholded for different coverages.

was full, and the dimension of the support was indistinguishable from the imbedding dimension.

The slope of the best fit line for the first decade distinctly decreases with decreasing coverage. Below 1.6% the curves are no longer linear probably owing to an insufficient number of events. The fractal dimension of the support of the image deduced from Fig. 6 varies from about 1.25 at 10% coverage to about 0.78 at 1.6%. Below 1.6% coverage the average slopes in Fig. 6 continue to decrease but the corresponding fractal dimension of the support is not less than 0.7.

The change in fractal dimension of the support across unity as the coverage varies from 10 to 1.6% is a most interesting result. It indicates that the distribution of the elements constituting the thresholded image has varied from one of corrugated lines to elaborated points. Presumably as the threshold was lowered the islands would gradually fill the 2-D space and the fractal dimension would approach 2. And as the threshold was continually raised the sparse remaining islands would resemble isolated points in space, and hence their fractal dimension would approach 0. Clearly the fractal dimension will be monotonically and inversely correlated with the nearest-neighbour distance.

The corresponding fractal dimension for the random surface is given by the extension of Eq. (14), and is arrived at by adding 1 to the fractal dimension of the thresholded sets. The fractal dimension of the surfaces varies from 2.25 to 1.7 as the threshold is raised and the areal coverage decreases from 10 to 0.1%. The results are presented in Fig. 7 for the 0.95- μm image of flight 7 for two decades of areal extent. The estimate of 2.25 indicates a fractal Brownian topography ($\alpha = 0.75$) whose texture is rather smoother than say Mandelbrot's mountains, in fact more like aged hills. Such a description ultimately fails, however. As the coverage is lowered and the fractal dimension falls to near 2 the implication is that the islands constituting the image become smoother, whereas in fact one might expect more internal variability in the light field. However, the mean distance between the islands also increases and the internal intensity variability is compromised by the greater inter-island variability. Eventually the description reduces to one dominated by the spacing between the islands. The fractal dimension approaches that of the support,

that is, the locations of the contorted shapes, being less influenced by any internal structure within the whitecaps.

It might be argued that it would be preferable to characterize the process by its Lipschitz exponent because it is a fractal property not dependent on the imbedding dimension. Its value is the same whether the entire 2-dimensional image or a 1-dimensional cut is analyzed. In this analysis the value of the exponent ranges from 0.75 to 1.3. However, it is more conventional to report the fractal dimension to conform with previously published estimates. In particular we note the general similarity of our result for the weakly fractal image with the estimate by Lovejoy (1982) of 2.35 for the fractal dimension of the surface of atmospheric clouds. We also re-emphasize that the estimate of fractal dimension decreases with the intensity of the scattered light from the whitecaps.

The decreasing fractal dimension with increasing intensity threshold violates the basic premise of the original analysis – that the fractal dimension is invariant to the range of intensity values. If Eq. (4) is applied conditionally in a range of intensity, say dI , near the minimum of I for apparent fractal behaviour, (in our case for intensities near 10% coverage) it should provide the same similarity exponent, α , as if the function was sampled over the same range, dI , near the maximal extreme, say near 0.1%, allowing that considerably longer original data series are required to achieve adequate statistical reliability. The implication of Figs 5 and 7 is that the process leading to the image distributes larger intensity events more erratically than lower intensity events. But all the events of differing intensities are fractal, if only weakly.

5 Discussion

A variation in fractal dimension within a sampled realization is consistent with recent developments in our understanding of non-linear dynamical processes (systems) such as turbulence. In this extended formulation of the concept of fractals it is postulated that there can exist within the overall process, here image, a subset of fractal identities, of differing fractal dimension, Lipschitz exponent and probability of occurrence.

Elsewhere (Kerman and Bernier, 1994) it is shown that the whitecap images are multifractal, with some subsets having implied fractal dimensions for their support as low as 0.3. Further the Lipschitz exponent of identifiable connected subsets (“islands”) forms a natural discriminator for the process to distinguish active entrainment in whitecaps ($\alpha < \alpha_c$) from the passive dissipation of foam patches ($\alpha > \alpha_c$) where α_c is a critical exponent. In addition, Schertzer and Lovejoy (1990) have likewise applied the technique to an analysis of the multifractal properties of clouds.

That the fractal dimension estimated by box counting, referred to in the literature as the covering dimension, varies with intensity threshold can be related to the image’s multifractal structure. Because the fractal dimension of a subset must be less than or equal to the fractal dimension of the imbedding set, it is only possible to

have a truly monofractal process if all the subsets are statistically identical. Therefore the fractal dimension that is estimated here for a given thresholded situation differs from that in a multifractal analysis. This arises because the probability of occurrence of various subsets of different α changes with the thresholding operation so that the fractal dimensions as estimated in this paper are weighted towards the fractal dimension of the more prevalent subsets.

What is clear on the basis of the analysis presented above, is that the images of a wind-swept sea, including the presence of foam and breaking waves, do reveal evidence of a fractal-like behaviour. Two methods, resolution reduction and box counting have shown the log-log ranges indicative of a self-similar fractal structure reasonably well. Indeed the nature of the fractal structure of the thresholded sets changes to point-like at a coverage of about 5% consistent with the maximum extent of fractal-like structure deduced from the degraded resolution analysis.

Acknowledgements

The authors would like to thank Bob Bloxam, Roy Mitchell and Joan Ryan for their dedicated help in various aspects of the data reduction and analysis during their different sojourns. The advice and assistance of various personnel at the Canada Centre for Remote Sensing, including Wally McCall, Bud McKibbin, George Fitzgerald, and last but not least, the flight crew, Bryan Healy, Andre Gignac, Gord Doucette and Bill Bayer. The authors wish to especially thank Shaun Lovejoy of McGill University for his patient advice while we struggled to understand fractal concepts in years past. We hope their efforts will now be seen in a larger and rewarding perspective.

References

- AUSTIN, R.W. and S. MORAN. 1974. Reflectance of whitecaps, foam and spray. Ocean color analysis. Visibility Lab., U. California San Diego, Scripps Inst. Oceanogr. Ref. 74-10.
- BLANCHARD, D.C. 1983. The production, distribution and bacterial enrichment of the sea salt aerosol. In: *The Air-Sea Exchange of Gases and Particles*, Reidel, pp. 407-454.
- BUAT MENARD, P. (Ed.). 1986. *The Role of Air-Sea Exchange in Geochemical Cycling*. Reidel.
- CROWTHER, P.A. 1980. Acoustical scattering from near-surface bubble layers. In: *Cavitation and Inhomogeneities in Underwater Acoustics*, W. Lauterborn (Ed.), Springer-Verlag.
- CSANADY, G.T. 1990. The role of breaking wavelets in air-sea transfer. *J. Geophys. Res.* **95**: 749-759.
- DAVIS, G.E. 1955. Scattering of light by an air bubble in water. *J. Opt. Soc. Am.* **45**: 572-581.
- FARMER, D. and S. VAGLE. 1989. Waveguide propagation of ambient sound in the ocean-surface bubble layer. *J. Acoust. Soc. Am.* **86**: 1897-1908.
- GLAZMAN, R.E. and P.B. WEICHMAN. 1989. Statistical geometry of a small surface patch in a developed sea. *J. Geophys. Res.* **94**: 4998-5010.
- HOLTHUIJSEN, L.H. and T.H.C. HERBERS. 1986. Statistics of breaking waves observed as whitecaps in the open ocean. *J. Phys. Oceanogr.* **16**: 290-297.
- KERMAN, B.R. 1984. A model of interfacial gas transfer for a well-roughened sea. *J. Geophys. Res.* **89**: 1439-1446.
- . 1986. On aerosol production and enrich-

- ment by breaking wind waves. *ATMOSPHERE-OCEAN*, **24**: 329-345.
- . (Ed.). 1988. *Sea Surface Sound*. Reidel.
- and L. BERNIER. 1994. Multifractal representation of breaking waves on the ocean surface. *J. Geophys. Res.* **99**: 16,179-16,196.
- KITAIGORODSKII, S.A. 1984. On the fluid dynamical theory of turbulent gas transfer across an air-sea interface in the presence of breaking wind-waves. *J. Phys. Oceanogr.* **14**: 960-972.
- KOEPKE, P. 1984. Effective reflectance of oceanic whitecaps. *Appl. Opt.* **23**: 1816-1824.
- LONGUET-HIGGINS, M.S. and N.D. SMITH. 1983. Measurement of breaking waves by a jump meter. *J. Geophys. Res.* **88**: 9823-9831.
- LOVEJOY, S. 1982. Area-perimeter relation for rain and cloud areas. *Science*, **216**: 185-187.
- MACINTYRE, F. 1968. A boundary-layer "microtome" for micron thick samples of a liquid surface. *J. Phys. Chem.* **72**: 589-592.
- MANDELBROT, B.B. 1983. *The Fractal Geometry of Nature*. Freeman.
- MONAHAN, E.C. and G. MACNIOCAILL (Eds). 1986. *Oceanic Whitecaps and Their Role in Air-Sea Exchange Processes*. Reidel.
- and I.G. O'MUIRCHARTAIGH. 1986. Whitecaps and the passive remote sensing of the ocean surface. *Int. J. Remote Sensing*, **7**: 627-642.
- and M.A. VAN PATTEN (Eds). 1989. Climate and health implications of bubble-mediated sea-air exchange. Symp. Proc., Conn. Sea Grant Publ. CT-SG-89-06.
- NOVARINI, J.C. and D.R. BRUNO. 1982. Effects of the sub-surface bubble layer on sound propagation. *J. Acoust. Soc. Am.* **72**: 510-514.
- PHILLIPS, O.M. 1985. Spectral and statistical properties of the equilibrium range in wind-generated gravity waves. *J. Fluid Mech.* **156**: 505-531.
- ROSS, D.B. and V. CARDONE. 1974. Observations of oceanic whitecaps and their relationship to remote measurements of surface wind speed. *J. Geophys. Res.* **79**: 444-452.
- ROTHROCK, D.A. and A.S. THORNDIKE. 1980. Geometric properties of the underside of sea ice. *J. Geophys. Res.* **85**: 3955-3963.
- SCHERTZER, D. and S. LOVEJOY. 1990. Nonlinear geodynamical variability: Multiple singularities, universality and observables. In: *Scaling, Fractals and Non-linear Geophysics II*, D. Schertzer and S. Lovejoy (Eds), Kluwer.
- SMITH, P.M. 1981. Measurements of whitecap coverage and surface winds over the Gulf of Mexico loop current. NORDA Rep. 43, Naval Ocean Res. Devel. Activity, NSTL Stn, Miss., 24 pp.
- SNYDER, R.L.; L. SMITH and R.M. KENNEDY. 1983. On the formation of whitecaps by a threshold mechanism: Part III. Field experiment and comparison with theory. *J. Phys. Oceanogr.* **13**: 1505-1518.
- THORPE, S.A. 1982. On the clouds of bubbles formed by breaking wind-waves in deep water, and their role in air-sea gas transfer. *Phil. Trans. R. Soc. Lond.* **A304**: 155-210.
- . 1986. Measurements with an automatically recording inverted echo sounder ARIES and the bubble clouds. *J. Phys. Oceanogr.* **16**: 1462-1478.
- TOBA, Y. and M. CHAEN. 1973. Quantitative expression of the breaking of wind waves on the sea surface. *Rec. Oceanogr. Works Jpn*, **12**: 1-11.
- WEISSMAN, M.; S.S. ATAKTURK and K.B. KATSAROS. 1984. Detection of breaking wave events in a wind generated wave field. *J. Phys. Oceanogr.* **14**: 1608-1619.
- WHITLOCK, C.H.; D.S. BARTLETT and E.A. GURGANUS. 1982. Sea foam reflectance and the influence of optimum wavelength for remote sensing of ocean aerosols. *Geophys. Res. Lett.* **9**: 719-722.
- ZWICK, H.; W.D. MCCOLL and H.R. EDEL. 1980. The CCRS DS1260 airborne multispectral scanner (MSS). Proc. 6th Can. Symp. Remote Sensing, Halifax, N.S., pp. 643-648.